Coherent wave reflection in integrable or chaotic symmetrical acoustical billiards

Victor Tyrode, Nicolas Totaro, Laurent Maxit, Alain Le Bot

PROCEEDINGS A

rspa.royalsocietypublishing.org

Research

Article submitted to journal

Subject Areas:
wave motion, acoustics, mechanics

Keywords:
random vibration, statistical energy analysis, diffuse field, coherent reflection, image-source

Author for correspondence:
Alain Le Bot
e-mail: alain.le-bot@ec-lyon.fr

THE ROYAL SOCIETY
PUBLISHING

Coherent wave reflection in integrable or chaotic symmetrical acoustical billiards.

V. Tyrode[1], N. Totaro[2], L. Maxit[2] and A. Le Bot[1]

[1]Univ Lyon, Ecole Centrale de Lyon, Laboratory of tribology and system dynamics, UMR CNRS 5513, 69134, Ecully, France
[2]Univ Lyon, INSA Lyon, LVA, EA677, 69621 Villeurbanne, France

This study is concerned with the distribution of flexural vibrations in plates excited with a Gaussian white noise. The distribution of energy can be characterized by its homogeneity and isotropy. Some particular geometries like the Bunimovitch stadium generate a field which is both homogeneous and isotropic. But other geometries produce a field which is homogeneous but not isotropic (like the rectangle panel) or non isotropic nor homogeneous (like the circular panel). It is known that these features drive the establishment of diffuse field. However, in the present work, we show that even at high frequency and for these three particular geometries, the diffuse field cannot be reached rigorously. Due to symmetries, the vibrational response is always enhanced on some particular lines and points by the effect of coherence between rays. The enhancement factors are predicted theoretically with the image source method. The presence of energy enhancement is also shown experimentally by measuring the vibrational energy density in the 20 Hz - 4 kHz frequency range for these three plates excited with a random white noise. Measurement of enhancement factors shows a good agreement with their theoretical predictions.

1. Introduction

Statistical energy analysis (SEA) is a theory of sound and vibration to predict the vibroacoustic response of structures in the high frequency range where classical methods like finite elements reach their limits [1].

SEA states that, under certain restrictive conditions [2,3], the vibrational energy of linear [4] or nonlinear oscillators [5] always flows from high to low levels of energy exactly like heat transfer [6–8]. In SEA, two adjacent subsystems may have different vibrational temperatures but must be individually in thermal equilibrium meaning that they have reached a state of diffuse field [9]. Applying a local energy balance, SEA predicts the vibrational energy in all subsystems.

At high frequency, the number of resonant modes (those which contribute significantly to the vibrational response) is large but this complexity is an advantage when applying a statistical approach like SEA. It is usually admitted that if the damping is low and the number of resonant modes is large in the subsystem, then the vibrational energy is uniformly distributed. This is the state of diffuse field which is one of the most important assumptions of SEA. More exactly, the diffuse field is usually defined as a homogeneous and isotropic superposition of plane waves whose phase is random. For that purpose, diagrams of validity of SEA in the frequency-damping domain have been proposed to predict the apparition of diffuse field [10,11].

However, high frequency and low damping are not sufficient conditions to ensure the diffuseness of the field [12]. The geometrical properties of the structure can lead to a non-homogeneity of the field [13,14]. In a circular plate which represents an example of integrable dynamical system, one can observe the presence of a caustic passing through the excitation point and where the energy density has a higher level [15]. Non-integrable system may exhibit a chaotic ray dynamics [16]. However, even if the dynamical system is chaotic, some effects can frustrate a perfectly uniform distribution of energy. The coherent backscattering effect [17,18] stems from constructive interferences of rays following reciprocal paths that always exist by virtue of the time-reversal symmetry. This energy enhancement is always observed on the source position [19]. Energy enhancement also exist on points and lines outside source position but for spatial symmetry reason [13,20,21]. This phenomenon has been observed for instance by deflectometry in Ref. [22].

The aim of this work is to study the enhancement factor of energy in vibrating plates with integrable shape (rectangle and circular) and chaotic shape (Bunimovitch stadium) [23,24] having a spatial symmetry. Firstly, theoretical results are obtained with the image source method. For this purpose, curved edges of stadium and circular plates are discretized in segments. Secondly, a direct numerical approach for predicting the location and strength of these intensifications is developed based on the modal expansion technique. Finally, experimental measurements by laser vibrometry are presented. Plates are excited with a shaker at high frequencies with a random white noise and measurements are compared with theoretical results.

2. Tested structures

One of the most important property of billiards is ergodicity. In an ergodic billiard, almost all rays pass through the vicinity of any point in any direction that is explore all points of the phase-space with the same probability. In the absence of constructive interference of rays, this particular propagation results in a homogeneous and isotropic vibrational field or, in other words, a diffuse field. But a spatial symmetry may induce constructive interferences between rays which frustrate the establishment of diffuseness. To explore all possible dynamics, we therefore chose shapes which combine ergodicity or not with spatial symmetries.

(a) Plate geometries

Three geometries are considered: a rectangular plate, a circular plate and a Bunimovitch stadium plate. These three shapes have been chosen because they are representative of the various behaviours in ray propagation of interest in SEA [25]. Furthermore, such simple geometries can be analyzed in terms of rays by the image source method to demonstrate the quantitative effect of coherent reflections that would have been difficult to provide in systems with more complex geometries.

The plates are made of stainless steel 430 with Young's modulus $E = 203$ GPa, mass density $\rho = 8010$ kg.m^{-3} and Poisson's ratio $\nu = 0.3$. The plates are 2 mm thick and their dimensions are represented in figure 1. Dimensions have been chosen so that all plates have the same area.

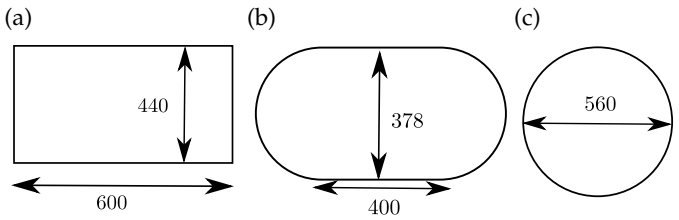

Figure 1. Dimensions of plates. (a); Rectangular, (b); Bunimovich stadium, and (c); circular plate.

(b) Ray propagation

These three shapes present different ray propagation patterns [26]. The top of figure 2 shows typical ray trajectories in these billiards after 100 reflections and the bottom shows the phase space structure for each billiard.

For the circular billiard, the dynamical system is integrable since the angular momentum is conserved (here defined as the sine of incidence angle) [27]. The ray turns in the circle bouncing on the boundary always with the same incidence angle. One can clearly observe the presence of a caustic which encloses a region of space never visited by the ray (figure 2a). Figure 2d shows that all points of the boundary are reached (although not all points enclosed by the circle) but also that not all values of angular momentum are reached (a single one is reached). Thereby ray propagation is neither homogeneous nor isotropic. Even if isotropy could be enforced by sending many rays in all directions (with a point source with a uniform directivity), the ray propagation will never reach homogeneity.

In the case of the Bunimovitch stadium billiard, the dynamical system is chaotic. The ray explores the whole phase-space with a uniform probability density of presence. In particular, a ray explores the vicinity of all points and spends equal times in regions of equal size (figure 2b). As it can be seen in figure 2e, the probability density function of presence is uniform in the phase-space.

The rectangular billiard is an intermediate case. Ray propagation is regular because the incidence angle on edges can take only two values. However, almost all rays entirely explore the spatial domain (but not the phase-space) as it can be seen in figure 2c. With a single ray, the resulting field is homogeneous, in contrast with the circular billiard, but not isotropic. Figure 2f shows that almost all rays entirely explore the spatial domain with a uniform probability in the position space. But there is only two values of angular moment reached by the ray. Therefore, even if the ray dynamics is not chaotic, the vibrational field may be diffuse by enforcing its isotropy with a large number of rays emmited by a point source with a uniform directivity.

3. Spatial distribution of energy

The objective of this section is to compute the local energy $E(x, y)$ of the previously described systems. Then, the nature of the vibrational field in the system is evaluated by comparing the energy at multiple points chosen at random.

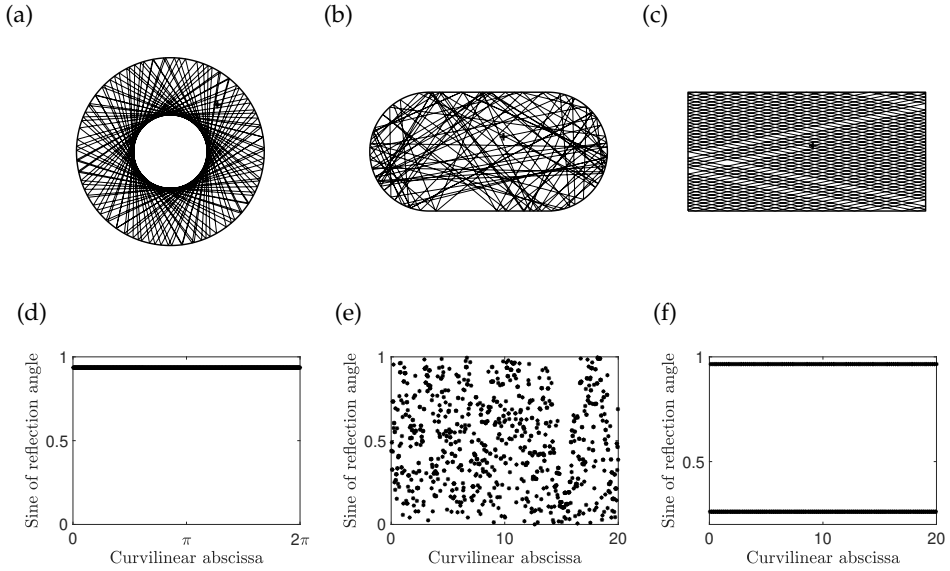

Figure 2. Ray propagation in the three tested structures with the phase space structure. (a,d); Circle, (b,e); Stadium, and (c,f); Rectangle.

(a) Local energy

The equation of motion governing the transverse deflection $u(x, y, t)$ of a damped plate excited in bending vibration by a time-varying normal force field $f(x, y, t)$ is

$$D\nabla^4 u(x, y, t) + \lambda \frac{\partial u}{\partial t}(x, y, t) + m\frac{\partial^2 u}{\partial t^2}(x, y, t) = f(x, y, t) \tag{3.1}$$

where $D = Eh^3/12(1 - \nu^2)$ is the bending stiffness, E the Young modulus, ν the Poisson ratio, h the plate thickness, $m = \rho h$ the mass per unit area, λ the viscous damping coefficient, and ∇^4 denotes the bilaplacian operator. The force field is a point force $f(x, y, t) = F(t)\delta(x - x_0))\delta(y - y_0)$ at x_0, y_0 where $F(t)$ is a stationary random process of constant power spectral density $S(\omega) = S_0$ in the angular frequency band $\Delta\omega$ centred on ω_c and zero elsewhere. Let H be the frequency response function between the vibrational velocity $\dot{u}(x, y, t)$ and the point force $f(x_0, y_0, t)$. The modal expension technique gives

$$H(x, y, x_0, y_0, \omega) = \sum_{n>0} \frac{\Psi_n(x_0, y_0)\Psi_n(x, y)}{m(\omega_n^2 - \omega^2 + j\eta\omega_n\omega)} \tag{3.2}$$

with Ψ_n the nth mode shape of the plate and $\eta = \lambda/(2m\omega_n)$ the damping loss factor. The natural frequencies ω_n and mode shapes Ψ_n are obtained by the finite element method using the MSC/NASTRAN 2021.1 code.

Let us first introduce the local vibrational energy. At any point (x, y) on the plate, the vibrational energy density is taken as twice the random expectation of the kinetic energy density $m\dot{u}^2(x, y, t)$,

$$E(x, y, \omega_c) = m < \dot{u}^2(x, y, t) > \tag{3.3}$$

where the probability expectation is noted with brackets and ω_c is added as variable in E to highlight the dependance on the centre frequency. Since the random force is stationary, the vibrational speed $\dot{u}$ is also stationary and the time no longer appears in the variables of E. In equation (3.3), $< \dot{u}^2(x, y, t) >$ is the auto-correlation $R_{\dot{u}\dot{u}}(\tau)$ of vibrational velocity taken at $\tau = 0$.

From the Wiener-Khinchin theorem,

$$< \dot{u}^2(x,y,t) >= R_{\dot{u}\dot{u}}(0) = \frac{1}{2\pi}\int_{-\infty}^{+\infty} S_{\dot{u}\dot{u}}(\omega)\mathrm{d}\omega \tag{3.4}$$

where $S_{\dot{u}\dot{u}}(\omega)$ denotes the power spectral density of $\dot{u}$. But $S_{\dot{u}\dot{u}}(\omega)$ is given by $S_{\dot{u}\dot{u}}(\omega) = \omega^2|H(x,y;x_0,y_0;\omega)|^2 S(\omega)$. Since the power spectral density is constant and equal to S_0 in the frequency band $\Delta\omega$ and zero elsewhere, the local vibrational energy at point (x,y) becomes

$$E(x,y,\omega_c) = \frac{mS_0}{\pi}\int_{\Delta\omega} \omega^2|H(x,y;x_0,y_0;\omega)|^2\mathrm{d}\omega \tag{3.5}$$

where an additional factor 2 appears by virtue of the fact that H is an even function. The calculation of energy field in a plate therefore reduces to the calculation of the receptance H in the frequency band $\Delta\omega$.

Let us comment the type of averaging appearing in the above equations. The brackets denote a random expectation that is an average over a large number of realizations of the stochastic process F. If the input process F is further assumed ergodic, then the random expectation is equal to the time average of a single realization of F (this assumption of ergodicity is not theoretically a requirement but is very convenient and useful in practice). Furthermore, equation (3.5) highlights the link between random expectation and frequency average. The integral of $S_{\dot{u}\dot{u}}$ over $\Delta\omega$ gives the energy of the signal $\dot{u}$ within the frequency band $\Delta\omega$. And for a white noise, the random expectation reduces to the frequency average of the square of the frequency response function H.

(b) Measure of field diffuseness

(i) Definition

The spatial distribution of energy can be characterised by the spatial average

$$\overline{E}(\omega_c) = \frac{1}{A}\int_A E(x,y,\omega_c)\mathrm{d}x\mathrm{d}y. \tag{3.6}$$

and, to estimate whether the field is diffuse or not, the standard deviation divided by the spatial average

$$\sigma(\omega_c) = \frac{1}{\overline{E}(\omega_c)}\sqrt{\frac{1}{A}\int_A (E(x,y,\omega_c) - \overline{E}(\omega_c))^2\mathrm{d}x\mathrm{d}y}, \tag{3.7}$$

where A is the plate area. The normalized standard deviation σ gives the relative fluctuations of energy on the plate surface. A high value of σ indicates that the vibration field is not uniform and that the field can not be considered as diffuse. Conversely, a low value of σ is an indication of the diffuseness of the field.

The normalized standard deviation σ defined here is linked to the so-called inverse participation ratio [28]. The inverse participation ratio is defined as the fourth-order moment of $\dot{u}$

$$I_p = \frac{\frac{1}{A}\int < \dot{u}^4(x,y,t) > \mathrm{d}x\mathrm{d}y}{(\frac{1}{A}\int < \dot{u}^2(x,y,t) > \mathrm{d}x\mathrm{d}y)^2} = \frac{\frac{1}{A}\int E(x,y,\omega_c)^2\mathrm{d}x\mathrm{d}y}{\overline{E}(\omega_c)^2}. \tag{3.8}$$

Comparing with (3.7), it follows immediately that $I_p = \sigma^2 + 1$ so that normalized standard deviation σ and inverse participation ratio I_p gives the same information.

(ii) Example of rectangular plate

In this section, the diffuseness of the vibratory field of a rectangular plate with free edges is evaluated using the normalised standard deviation defined in equation (3.7). The numerical process described in section (a) is applied to evaluate the local energies. The expectation of local energy is estimated by equation (3.5) at 7000 receiver points chosen at random. The integration over frequency is computed on 16 frequency bands Δf from [20-63] Hz, [20-125] Hz, ..., to [20-8000] Hz. The lower limits $f_{\min}$ of all the frequency bands are set to the same value 20 Hz whereas

the upper limits $f_{\max}$ are logarithmically spaced between 63 Hz and 8000 Hz. In addition, 30 damping loss factor values are considered, varying from 0.001 to 1, evenly spaced on a log scale. The integral in equation (3.5) is approximated using the rectangle rule. The angular frequency step is chosen as $\delta\omega = 2\pi f_{\min}\eta/4$ with η the damping loss factor, the same for all modes.

Figure 3 represents the map of the relative spatial standard deviation in the frequency-damping loss factor plane for a rectangular plate with dimensions presented in figure 1. The x-axis represents the higher frequency for each frequency band. The structure is excited at $x_0 = 0.22$ m and $y_0 = 0.12$ m with a point force having a constant power spectral density in the frequency band. The contour lines represent constant values of σ.

The map of figure 3 highlights that it exists three different states of a vibrational field. These are visible around points A, B and C represented by crosses. Figure 4 shows examples of simulated vibrational fields in the rectangular plate for the three configurations corresponding to point A, B and C. The energy is presented in dB. The vibratory states at these points can be characterized by:

- Point A is characteristic of a *modal field* with σ greater than 1. The frequency integration band is [20-63] Hz and the damping loss factor is equal to 0.002. As shown in figure 4a, the response of the plate is dominated by one or few modes so that the distribution of vibrational energy is highly fluctuating due to the existence of modal lines. The region of modal field is confined to low frequencies in the frequency-damping loss factor plane.
- Point B is characteristic of a *direct field* with σ is greater than 2. The frequency integration band is [20-4000] Hz and the damping loss factor is equal to 0.2. In this regime, the propagation of rays is limited to few reflections because the damping being very high their energy decreases quickly. This is the regime where reverberation is negligible and the vibrational field is circular in the vicinity of source (see figure 4b). The region of direct field is confined to high frequencies and high damping in the frequency-damping loss factor plane.
- Point C is characteristic of a *diffuse field* and is localized into the region delimited by the contour line $\sigma = 0.6$. The frequency integration band is [20-4000] Hz and the damping loss factor is equal to 0.002. In this regime, each point of the plate receive approximately the same level of energy. At a first approximation, the vibrational field can be considered as spatially homogeneous and isotropic (see figure 4c). The region of diffuse field is confined to high frequencies and low damping in the frequency-damping loss factor plane [2].

(c) Highlighting of local energy enhancement

We now further explore the diffuse field region for the two other shapes. Vibrational energy simulations are also done for the circular and stadium shaped plates. The frequency integration band is [20-4000] Hz and the damping loss factor is equal to 0.002. These values are associated to point C in the previous section that corresponds to a diffuse field. Figure 5 shows the simulated vibrational energy fields in these plates.

It may be observed that a diffuse field appears on both the rectangular (figure 4c) and stadium shaped plates (figure 5a). This is confirmed by the standard deviation σ which is equal to 0.54 for the rectangular plate and 0.31 for the stadium plate. However, even if the distribution of energy is considered as diffuse the vibrational field is not fully spatially homogeneous due to the effect of rays coherence. The energy distribution exhibits patterns with enhancement. From these numerical simulations, enhancement factors are calculated as the vibrational energy on these patterns divided by the background diffuse energy. The numerical values of enhancement factors are determined for the rectangular, stadium shaped, and circular plates and are presented in table 1. Uncertainties are estimated with the standard deviation.

For the rectangular plate (figure 4c), the lines of intensified response form a tic-tac-toe pattern with the driving point at one of the four intersections. The enhancement factor on these four lines (d_i) is determined by averaging vibrational energy for all the points located on these lines and is

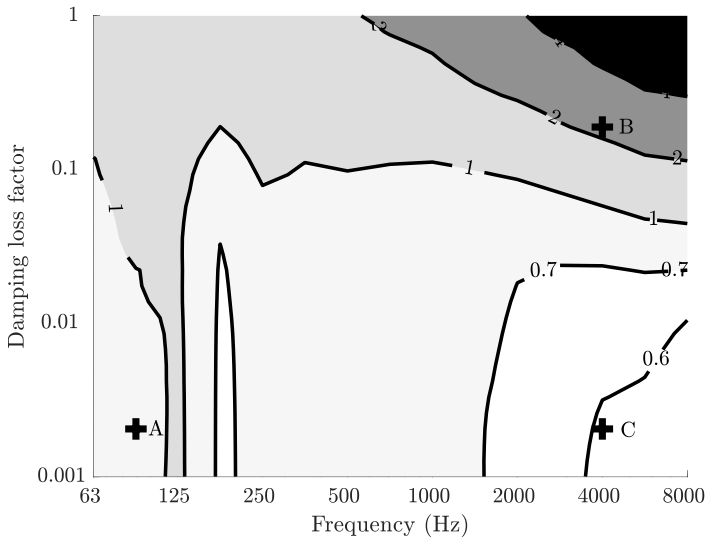

Figure 3. Relative standard deviation of spatial energy distribution in the frequency-damping loss factor plane for a rectangular plate with free edges under a point excitation.

equal to 1.31. Regarding the four points at lines intersections (S_i) the enhancement factor is equal to 3.48.

In the same way, for the stadium shaped plate (figure 5a), four points of energy enhancement are clearly visible due to two spatial symmetries with respect to vertical and horizontal lines. With the same method as before, the enhancement factor at these four points is determined and is equal to 3.07.

For the circular plate (figure 5b), vibrational energy never reaches a state of diffuse field and $\sigma = 2.81$ which is much higher than 0.6. Energy is higher along the circle passing through the excitation point as shown in figure 5b. This energy enhancement along this circle can be explained with geometrical acoustics in its strict sense that is without taking into account a phase in rays. As shown in figure 2a, all rays have a caustic along which the energy is higher. So the enhancement of energy on the source circle in the presence of multiple rays is due to a geometrical focusing of rays but not to a phenomenon of ray coherence. However, it can also be seen in figure 5b that the vibrational energy is also higher on the diameter passing through excitation point. But this time, the enhancement is due to the coherence of rays induced by the spatial symmetry. From numerical simulation, the factor of enhancement observed on this diameter is equal to 2.70. As the vibrational field is not diffuse, the error is larger than for the others.

These enhancement factors are theoretically calculated in the next section.

4. Quantification and localisation of local energy enhancement

The source image technique is the appropriate tool for determining the patterns of enhanced energy for the three studied plates. This method is particularly helpful in providing clear insight into the location and relative intensification of zones of enhanced energy. For the sake of simplicity, these properties are established without taking into account the attenuation. By analogy with geometrical acoustics, the propagation of waves can be considered in the form of rays emerging from the source point and image sources obtained by symmetry of the actual source with plate edges [29].

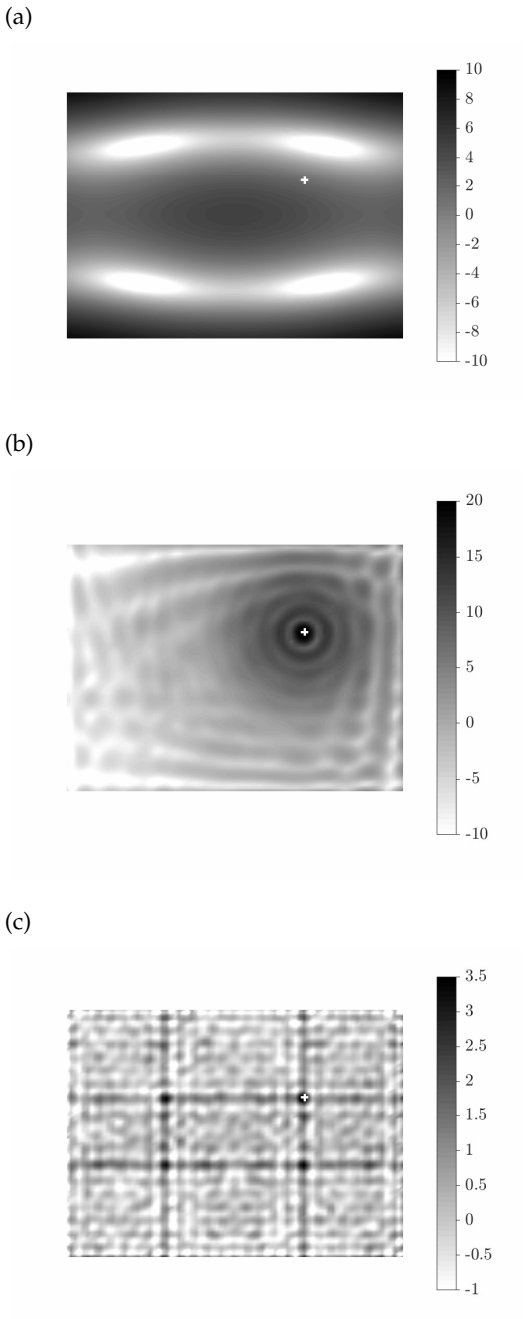

Figure 4. Vibrational energy distribution (in dB) computed with the eigenmodes in the rectangular plate with free edges. (a): modal field (Δf=[20-63] Hz, η=0.002), (b): direct field (Δf=[20-4000] Hz, η=0.2), and (c): diffuse field (Δf=[20-4000] Hz, η=0.002). The actual point force position is represented with a cross.

(a) Rectangular plate

Figure 6 shows the pattern of image sources in the rectangular plate of length L_x and width L_y.

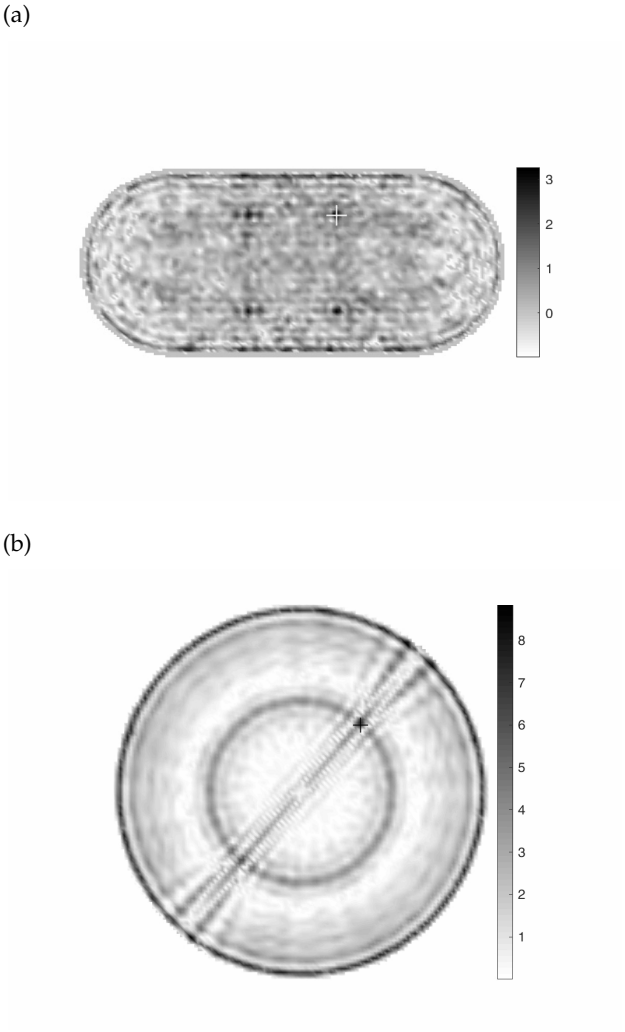

Figure 5. Vibrational energy distribution (dB) computed with the eigenmodes for the stadium (a) and the circular plate (b) excited by a point force (Δf=[20-4000] Hz and $\eta = 0.002$). The cross indicates the force position.

The actual source where the force is applied is located at point $S_0(x_0, y_0)$. We first introduce the points $S_1(x_0, L_y - y_0)$, $S_2(L_x - x_0, y_0)$, $S_3(L_x - x_0, L_y - y_0)$ and the lines $d_0(x = x_0)$, $d_1(x = L_x - x_0)$, $d_2(y = L_y - y_0)$, and $d_3(y = y_0)$ where enhancement is observed. The 15 image sources ($A, B, ...,$ to D_3, C_3) are obtained by applying successive symmetries with respect to the plate edges. Of course, an infinite number of image sources does exist but these 16 image sources are sufficient for this illustration. To estimate the intensification on points S_1, S_2, and S_3 and lines d_0 to d_3, we need to know the fraction of incoming waves that can be grouped into pairs of waves with identical response. If we consider the contribution to the response from a single uncorrelated wave of the source group A, B, C, D, to be $1/4$, the contribution from the group to a non special point of the rectangular plate is equal to 1. First, we note that point C_2 and D_2 are symmetric to C and D with respect to line d_2. So, at any point on d_2 (J for example), the wave arriving from C (resp. D) is identical to the wave arriving from C_2 (resp. D_2). At point J, waves arriving from A and B are uncorrelated with any other so their contribution is $\frac{1}{4}(1)^2$ where the square remind

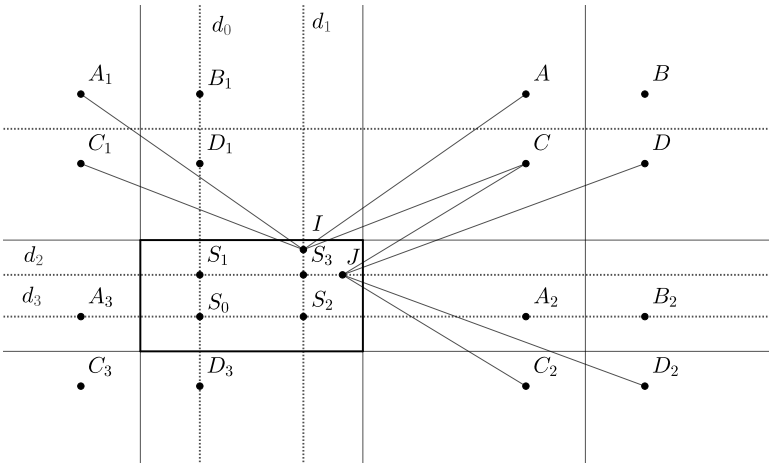

Figure 6. Lines $(D_0, ..., D_3)$ and points $(S_0, ..., S_3)$ of intensified response on rectangular plate excited at S_0 with symmetrically placed image sources.

that we sum energies. The contribution from C and C_2 (resp. D and D_2) is $\frac{1}{4}(1+1)^2 = 1$ and so the contribution from C (resp D) is $\frac{1}{2}$. Finally the contribution from the group A, B, C, D is equal to $\frac{1}{4} + \frac{1}{4} + \frac{1}{2} + \frac{1}{2} = \frac{3}{2}$. For the same reason, the enhancement factor is also $\frac{3}{2}$ for lines d_0, d_1 and d_3.

At the intersection S_3 of line d_1 and d_2, the wave arriving from A is doubled with the ray arriving from A_1, the wave arriving from D is doubled with the ray arriving from D_2, the wave arriving from C is quadrupled with rays arriving from C_1, C_2, and C_3 and the wave from B is uncorrelated with any other wave. The relative intensification at point S_3 is $\frac{1}{4}(\frac{1}{2}(1+1)^2 + \frac{1}{2}(1+1)^2 + \frac{1}{4}(1+1+1+1)^2 + 1) = \frac{9}{4}$. For the same reason, the enhancement factor is also $\frac{9}{4}$ at points S_1 and S_2.

Table 1. Comparison between numerical and theoretical enhancement factors for the three plate

	Theoretical (linear)	Theoretical (dB)	Numerical (dB)	Error (%)
Rectangle (S_i)	9/4	3.52	3.48± 0.2	1.13
Rectangle (d_i)	3/2	1.76	1.31± 0.7	25.5
Stadium	2	3.01	3.07± 0.1	1.99
Circle	2	3.01	2.70± 1.4	10.29

Similar analyses are done in Ref. [20] for special source positions for both rectangular and square plates. The square presents more symmetries than the rectangle and this results in the generation of other high energy lines. Furthermore, the enhancement factor generally increases with the number of symmetries.

It is important to notice that a modification of boundary conditions can lead to a change of the enhancement factors. When a plane wave hits a boundary, it is subjected to a phase shift. In the simply supported case, the phase shift is equal to π for all incidences but if the boundary is free or clamped, the phase shift depends on the incidence angle [30]. If the boundary conditions are not uniform and break down the spatial symmetry of the rectangle, rays no longer interfere constructively. It is even possible that for special combinations of phase shifts, rays interfere destructively leading to an enhancement factor smaller than one.

(b) Stadium shaped plate

Figure 7 shows the stadium shaped plate with the source located at $S_0(x_0, y_0)$ and 7 image sources $A_1, A_2, ..., C_2, D$. Curved elements of the stadium are segmented with lines Δ_1, Δ_2, ... to obtain plane surfaces. Then, image sources are determined by successive symmetries with respect to the plate edges. For example, image source B_1 (resp. C_1) is the symmetric of S_0 with respect to Δ_1 (resp. Δ_2). We consider the contribution to the response from the source group A_1, B_1, C_1 and D. In the same way as for the rectangular plate, rays arriving from A_1, B_1 and C_1 are respectively correlated with rays arriving from A_2, B_2, and C_2 at point S_1. Their contribution is $\frac{1}{2}(1+1)^2\frac{1}{4}$. Ray arriving from D is uncorrelated with any other so the contribution is $\frac{1}{4}(1)^2$. For the group A_1, B_1, C_1, and D, the contribution at point S_1 is:

$$3 \times \frac{1}{2}(1+1)^2\frac{1}{4} + \frac{1}{4}(1)^2 \tag{4.1}$$

To get an asymptotic estimation, let us extrapolate with n image sources. At point S_1, the contribution from the n images source is:

$$(n-1) \times \frac{1}{2}(1+1)^2\frac{1}{n} + \frac{1}{n} \tag{4.2}$$

As n approaches infinity, equation (4.2) approaches 2. Then, the intensification factor at point S_1 for a stadium is 2. In the same way, the intensification factor at points S_3 and S_2 is also 2. In this case, the intensification factor is obtained with an odd number of edges. This results remains unchanged if we considered an even number of edges since the term $1/n$ approaches 0.

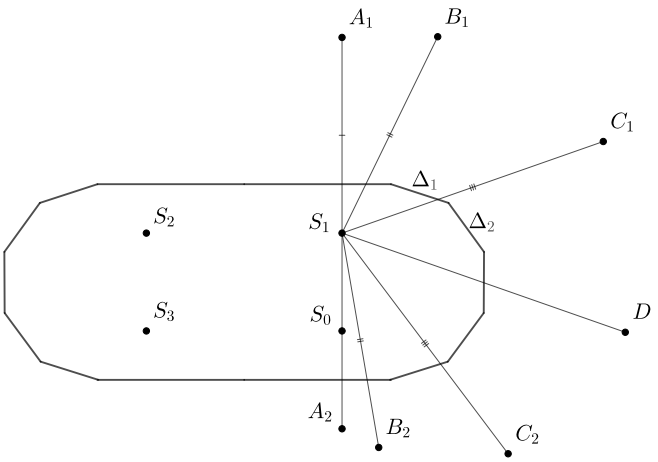

Figure 7. Points of intensified response $S_0, ..., S_3$ on stadium plate excited at S_0 with symmetrically placed image sources ($A_1, A_2, ..., C_2, D$).

(c) Circular plate

Figure 8 shows a representation of a circular plate which has been discretised. The source S_0 and 7 image sources $A_1, A_2, ..., C_2, D$ are obtained by successive symmetries with respect to the edges. As an example, the image source A_1 is the image of source S_0 by symmetry with respect to the boundary Δ_1. Consider the contribution to the response from the source group A_1, B_1, C_1 and D_1. Rays arriving from A_1, B_1 and C_1 are respectively correlated with rays arriving from A_2, B_2 and C_2 along the line D_0. Their contribution is $\frac{1}{2}(1+1)^2\frac{1}{4}$. Ray arriving from D_1 is uncorrelated with any other so the contribution is $\frac{1}{4}(1)^2$. For the group A_1, B_1, C_1 and D_1, the contribution at

point S_1 is:

$$3 \times \frac{1}{2}(1+1)^2 \frac{1}{4} + \frac{1}{4}(1)^2 \tag{4.3}$$

When we extrapolate, the contribution to point S_1 from n images source is:

$$(n-1) \times \frac{1}{2}(1+1)^2 \frac{1}{n} + \frac{1}{n} \tag{4.4}$$

With a similar reasoning as for the stadium shaped plate, the intensification factor along the line D_0 approaches 2 as the number of image sources goes to infinity.

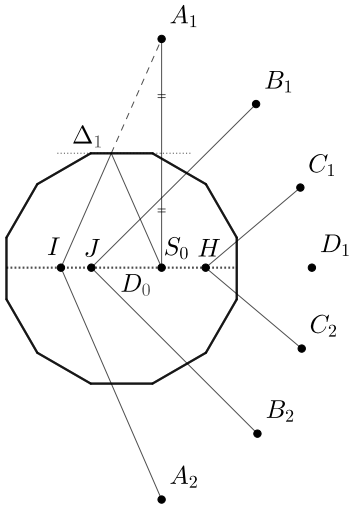

Figure 8. Line of intensified response D_0 on circular plate excited at S_0 with symmetrically placed image sources.

(d) Comparison with numerical results

Table 1 presents a comparison between the enhancement factors for the three plates determined by both the image-source method (theoretical values) and direct numerical simulation (numerical values) of Section (c).

There is a good agreement between numerical and theoretical values. However the numerical values are slightly lower than theoretical ones. This can be attributed to the effect of energy dissipation by structural damping which tends to reduce the enhancement and which is not taken into account in the theoretical approach. Numerical simulations are also limited to a frequency band due to computing capabilities and therefore the computed energy is truncated. Even if this band is wide, this limitation can affect the result.

5. Experimental investigation

(a) Experimental setup

In this section, we present measurements of the energy field for the three different geometries. The experimental setup is shown in figure 9. The plate is suspended from a rigid frame with two bungee cords attached to the plate top by small holes. A shaker (PCB K2004E01) is suspended from the rigid frame and linked to the plate by a stinger bonded with an epoxy glue. The shaker

applies a random vibration to the plate. The plate response is measured at multiple points with a laser vibrometer PSV500 with a scanning head. From the PSV software, the plates are meshed with 1200 points for the rectangular plate, 2400 points for the circular plate, and 1236 points for the stadium shaped plate.

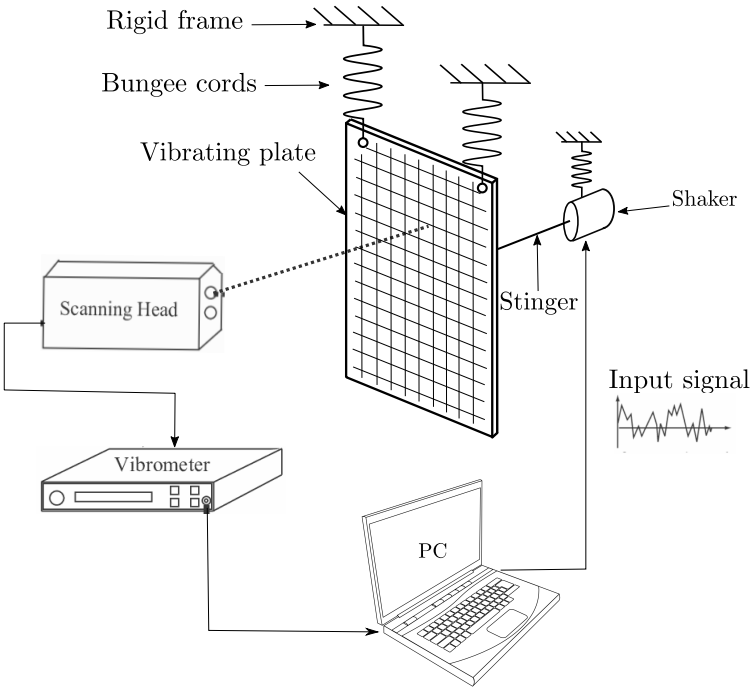

Figure 9. Experimental setup. The shaker excites the plate (meshed with 1200 points) through the stinger which is bonded on the plate. The response is measured with the scanning head and the vibrometer.

To verify that the shaker does not modify the plate behaviour, the first four natural frequencies measured with the laser vibrometer are compared with those obtained by numerical simulation with a finite element model. Results are summarized in table 2. The error is small, demonstrating that the presence of the shaker do not modify the normal modes of the plate. Moreover, at 4 kHz, the wavelength is 71 mm which is much higher compared to the diameter of the holes so that their influence is negligible.

Plates are excited with a Gaussian white noise in the frequency band 10 Hz - 8 kHz with an input voltage of 0.1 V. At each point the velocity is measured and filtered with a Hamming

Table 2. Comparison between numerical and experimental natural frequencies for the rectangular plate

Simulation (Hz)	Experiment (Hz)	Error (%)
26.14	26.69	2.08
59.19	60.94	2.95
76.04	79.04	3.94
89.62	88.09	1.81

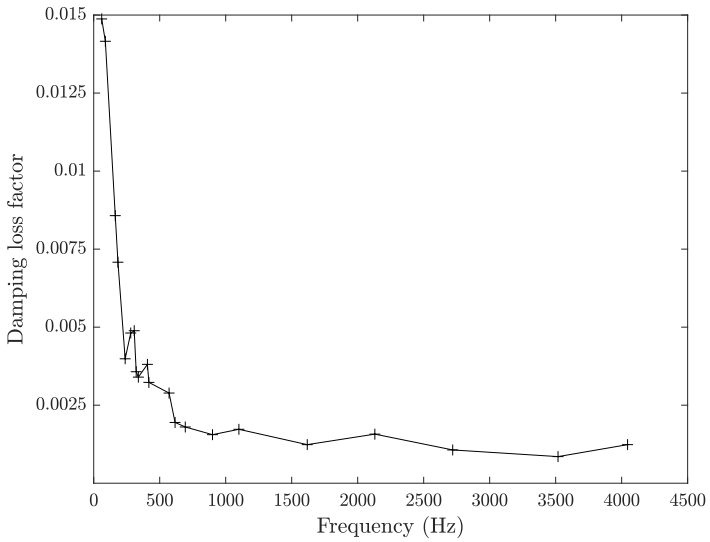

Figure 10. Evolution of damping loss factor

window between 20 Hz and 4 kHz. The power spectral density of the source is flat in the frequency band.

In order to estimate the expected distribution of energy in the rectangular plate using the map presented in figure 3, the damping loss factor is estimated at different natural frequencies with the half-power bandwidth method. Figure 10 presents the evolution of damping loss factor in the rectangular plate when the frequency increases. The damping decreases quickly to a value lower than 0.002 from 600 Hz to 4000 Hz. The measurements are performed at point C of figure 3 and therefore a nominally diffuse field is expected.

Finally, a Fourier transform of the vibrational velocity is estimated with a resolution of 6400 points by averaging 20 measurements and the mean vibrational energy is calculated with the integration bounds limited from 20 Hz to 4 kHz.

(b) Results

Figure 11 shows the vibrational energy distribution in the three plates in dB. Lines and points of intensified response are clearly visible. From these results, it is possible to measure enhancement factors. Table 3 presents a comparison between experimental and theoretical enhancement factors for the three plates. First, the background diffuse energy is estimated by taking the spatial average of the vibrational energy outside area of intensified response. Then, for the circular and

rectangular plates, the enhancement factor on the lines is determined by averaging vibrational energy for all the points located in the vicinity of these lines and divided by the background diffuse energy. The same procedure is applied for the four points with higher energy in the stadium shaped plate and rectangular plate.

Experimental measurements are always slightly below theoretical values but this is an expected results because damping loss factor of plates are not taken into account with the source image method. Moreover, the difference with theoretical results can be explained taking into account the measurements uncertainties like Young's modulus and the mass density which can slightly differ from their theoretical values. Also the excitation point is not perfectly punctual in practice due to the bonding and the boundary conditions are also not absolutely perfect.

Table 3. Comparison between experimental and theoretical enhancement factors for the three plate. Uncertainties are estimated with the standard deviation.

	Theoretical (dB)	Experimental (dB)	Error (%)
Rectangle (S_i)	3.52	3.0 ± 0.2	14.7
Rectangle (D_i)	1.76	1.5 ± 0.2	14.7
Stadium	3.01	2.7 ± 0.1	9.96
Circle	3.01	2.9 ± 0.6	3.65

6. Conclusion

In the present work, we have shown that high frequencies and low damping are not enough to ensure a perfect diffuse field. Geometrical properties of subsystems are important and are responsible for the presence of energy enhancement at points different from the source. The Bunimovich stadium presented is a good example because even if it is a chaotic system, the energy field is not totally diffuse and four points with a higher energy have been observed. Lines of energy enhancement have also been observed for rectangular and circular plates. With the image source method, enhancement factors have been determined for the three plates. Measurements of energy density level with a laser vibrometer have been realized and a good agreement is found with results obtained with image source method.

The practical applications of these results are of interest in SEA theory. Indeed, even if the system is chaotic, a great attention must be paid to the diffuseness of the vibrational field to strictly respect the SEA assumptions. If two subsystems are coupled in the vicinity of a point presenting an energy enhancement, the vibrational field can no longer be considered as diffuse at that point. We may expect that the exchange of vibrational power will be driven by the local level of energy and not the level of diffuse background. This would result in a deviation with the standard law of SEA which states that the exchange power is proportional to the difference of modal energies. So the actual exchange of energy will differ from the value predicted by SEA. This phenomenon has been observed in Refs. [2,25]. Stricly speaking, SEA is the statistical theory of sound and vibration which requires that all subsystems are in thermal equilibrium [8].

Data Accessibility. Experimental data and Matlab scripts to generate figures of numerical simulations are released as the electronic supplementary material.

Authors' Contributions. The ideas presented in this article have been put forward and debated by all authors. V.T. and N.T. have contributed to program the numerical examples and conducted the experiments. All authors have contributed to write the manuscript, and gave final approval for publication.

Competing Interests. We have no competing interests.

Funding. The authors are grateful for the financial support of the Up2HF project from Institut Carnot Ingénierie@Lyon. This work was also performed within the framework of the LABEX CeLyA (ANR-10-LABX-0060) of Université de Lyon, within the program « Investissements d'Avenir » (ANR-16-IDEX-0005) operated by the French National Research Agency (ANR).

Acknowledgements.

References

1. Le Bot A. 2015 *Foundation of statistical energy analysis in vibroacoustics*. Oxford University Press.
2. Lafont T, Totaro N, Le Bot A. 2014 Review of statistical energy analysis hypotheses in vibroacoustics. *Proc. R. Soc. A* **470**, 20130515.
3. Lafont T, Totaro N, Le Bot A. 2017 Coupling strength assumption in statistical energy analysis. *Proc. R. Soc. A* **470**, 20130515.
4. Mace B, Ji L. 2007 The statistical energy analysis of coupled sets of oscillators. *Proc. R. Soc. A* **463**, 1359–1377.
5. Spelman G, Langley R. 2015 Statistical energy analysis of nonlinear vibrating systems.. *Phil.Trans.R.Soc.A* **373**, 2051.
6. Le Bot A. 2009 Entropy in statistical energy analysis. *J. Acoust. Soc. Am.* **125**, 1473–1478.
7. Le Bot A., Carcaterra A. MD. 2010 Statistical vibroacoustics and entropy concept. *Statistical Vibroacoustics and Entropy Concept* **125**, 1473–1478.
8. Le Bot A. 2017 Entropy in sound and vibration: towards a new paradigm. *Proc. R. Soc. A* **473**, 20160602.
9. Le Bot A. 2007 Derivation of statistical energy analysis from radiative Exchanges. *J. Sound Vib.* **300**, 763–779.
10. Le Bot A, Cotoni V. 2010 Validity diagrams of statistical energy analysis. *J. Sound Vib.* **329**, 221–235.
11. Le Bot A, Bazari Z, Klein P, Lelong J. 2017 Statistical analysis of vibration in tyres. *J. Sound Vib.* **392**, 187–199.
12. Catheline S, Gallot T, P. Roux, G. Ribay, J. de Rosny. 2011 Coherent backscattering enhancement in cavities. *Wave Motion* **48**, 214–222.
13. Crandall SH. 1980 Localized response reductions in wide-band random vibration of uniform structures. *Ing. arch* **49**, 347–359.
14. Crandall SH, Zhu W. 1986 Wide band random vibration of an equilateral triangular Plate. *Probabilistic Engineering Mechanics* **1**, 5–12.
15. Itao K, Crandall SH. 1978 Wide-band random vibration of circular plates. *Journal of Mechanical Design* **100**, 690–695.
16. Tanner G, Søndergaard N. 2007 Wave chaos in acoustics and elasticity. *J. Phys. A: Math. Theor.* **40**, R443–R509.
17. Larose E, Lobkis OI, Weaver RL. 2006 Coherent backscattering of ultrasound without a source. *Europhys. Lett.* **76**, 422–428.
18. Weaver R, Yoritomo J. 2017 Diffuse elastic waves in a nearly axisymmetric body: Distribution, transport, and dynamical localization. *The Journal of the Acoustical Society of America* **141**, 3746–3746.
19. Weaver R, Lobkis O. 2000 Enhanced Backscattering and Modal Echo of Reverberant Elastic Waves. *Phys. Rev. Lett.* **84**, 4942–4945.
20. Langley AJ, Taylor. 1979 Chladni patterns in random vibration. *International Journal of Engineering Science*.
21. Elishakoff I, Ducreux B. 2014 Dramatic Effect of Cross-Correlations in Random Vibration of Point-Driven Spherically Curved Panel. *Arch Appl Mech* **84**, 473–490.
22. Le Bot A, Robin O, Rouard K, Berry A. 2021 Analysis of random mechanical vibrations in symmetrical thin plates using full-field vibration measurements. *Journal of Vibration and Acoustics* **143**, 024503.
23. Wright M, Weaver R. 2010 *New directions in linear acoustics and vibration: Quantum Chaos, Random Matrix Theory and Complexity*. Cambridge University Press.
24. Tanner G. 1997 How chaotic is the stadium billiard? A semiclassical analysis. *J. Phys. A: Math. Gen.* **30**, 2863–2888.
25. Li H, Totaro N, Maxit L, Le Bot A. 2019 Ergodic billiard and statistical energy analysis. *Wave Motion* **87**, 166–178.

26. Stöckmann HJ. 1999 *Quantum chaos: an introduction*. Cambridge [England] ; New York: Cambridge University Press.
27. Sondergaard N, Tanner G. 2002 Wave chaos in the elastic disk. *Phys. Rev. E* **66**, 066211.
28. Biddle J, Priour DJ, Wang B, Das Sarma S. 2011 Localization in one-dimensional lattices with non-nearest-neighbor hopping: Generalized Anderson and Aubry-André models. *Phys. Rev. B* **83**, 075105.
29. Polack J. 1993 Playing billiards in the concert hall: The mathematical foundations of geometrical room acoustics. *Applied Acoustics* **38**, 235–244.
30. Graff K. 1991 *Wave Motion in Elastic Solids*. Dover Books on Physics Series. Dover Publications.

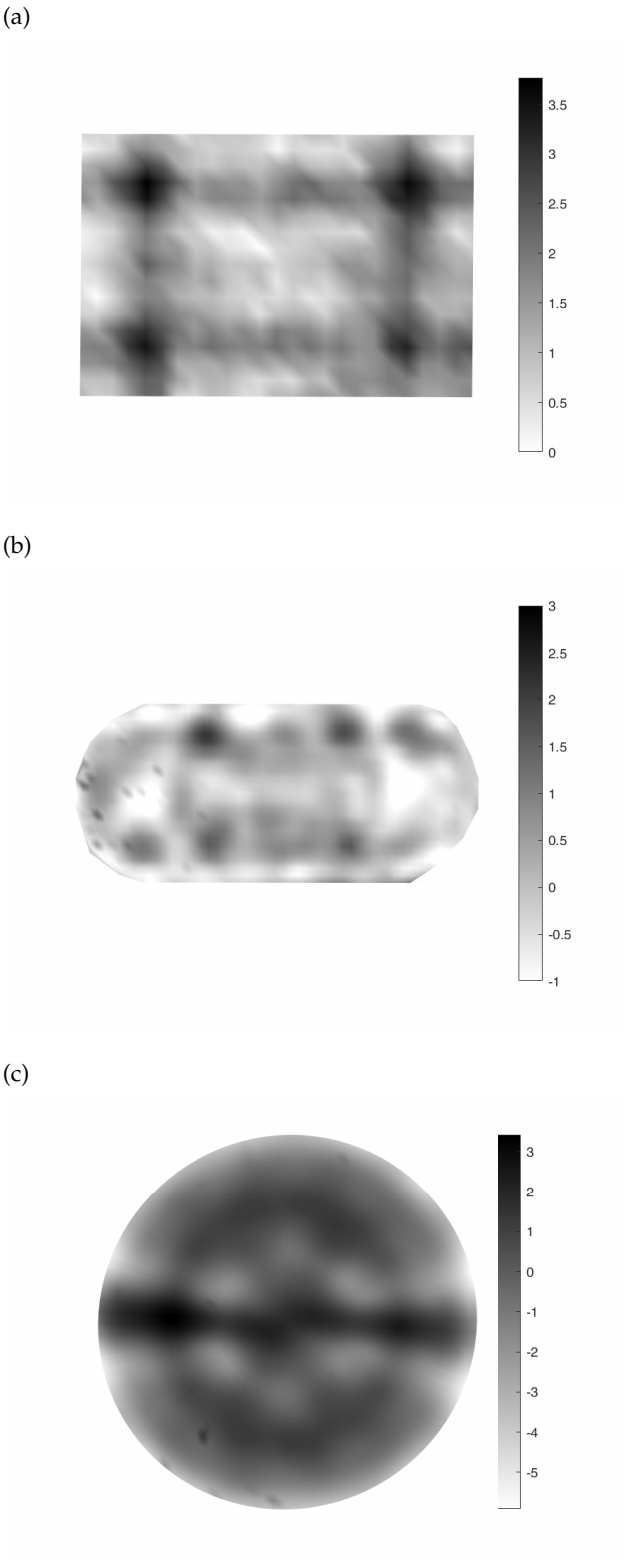

Figure 11. Distribution of energy density level (dB) for the three plates excited by a point force.